Supporting Information

Highly luminescent N-doped carbon quantum dots from lemon juice with porphyrin-like structures surrounded by graphitic network for sensing applications

*Tapas Kumar Mondal[a], Abhisek Gupta[a], Bikash Kumar Shaw[a], Supriya Mondal[a,b], Uttam Kumar Ghorai[c] and Shyamal K. Saha[a]**

E-mail: cnssks@iacs.res.in
*[*a]Department of Materials Science, Indian Association for the Cultivation of Science Jadavpur, Kolkata, 700032, India*
[b] Department of Physics, P.R Thakur Govt.College,Thakurnagar,Gaighata, North 24 parganas - 743287, India
[c] Department of Industrial Chemistry and Applied Chemistry, Swami Vivekananda Research Center, Ramakrishna Mission Vidyamandira, Belur math, Howrah-711202, India

Table of contents in Supporting Information:

23. **Table S1:** Stabilization energies of bare and ion incorporated NCQD core with their optimized geometrical parameters:

24. **Table S2:** Relative standard deviations (RSD) of various metal ions:

1. Synthesis procedure of exsitu NCQD:

0.5g citric acid and 0.11g ascorbic acid were dissolved in 20ml distilled water and maintained pH-8 using ammonia then the mixture was transferred into autoclave and take it at 180°C for 6 hours. After the reaction, brown coloured solution was filtered through 0.22µm Millipore filter papers and dialysed through dialysis tube (1KDa) for 24 hours.

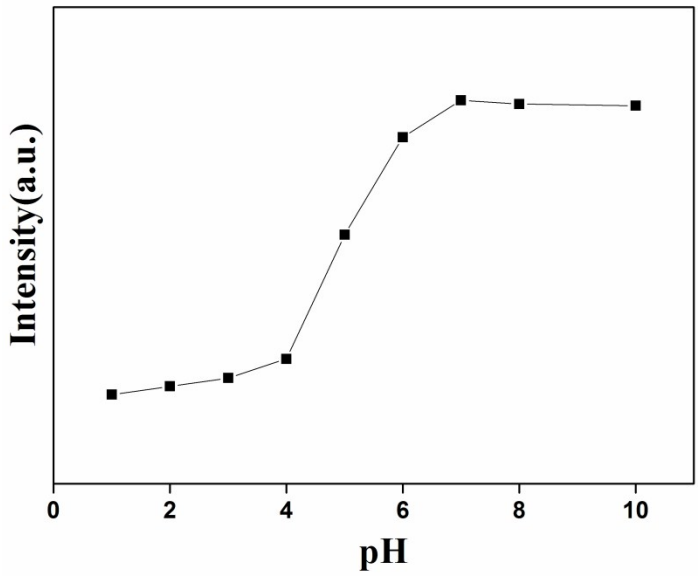

Figure S1: pH dependent PL spectra of NCQD

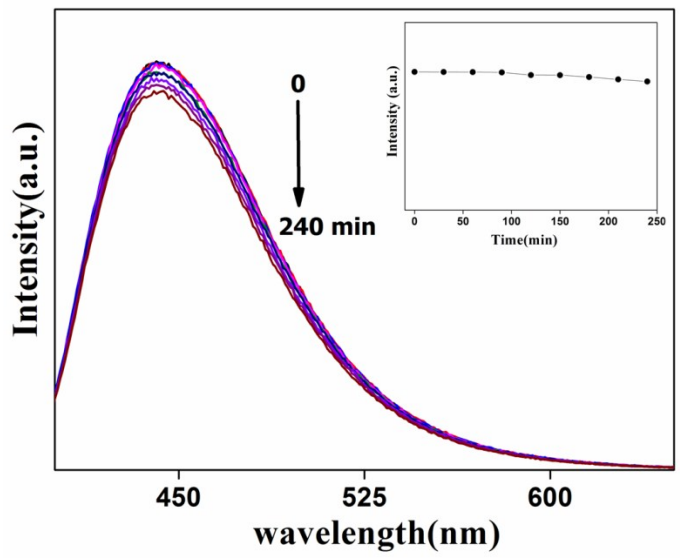

Figure S2: Time dependent PL spectra of NCQD

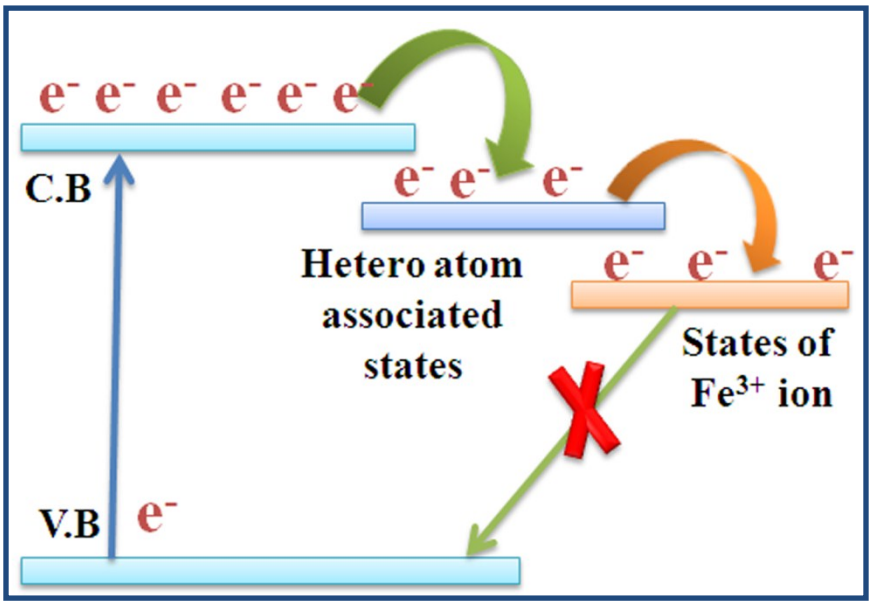

Figure S3: Probable scheme of dynamic PL quenching

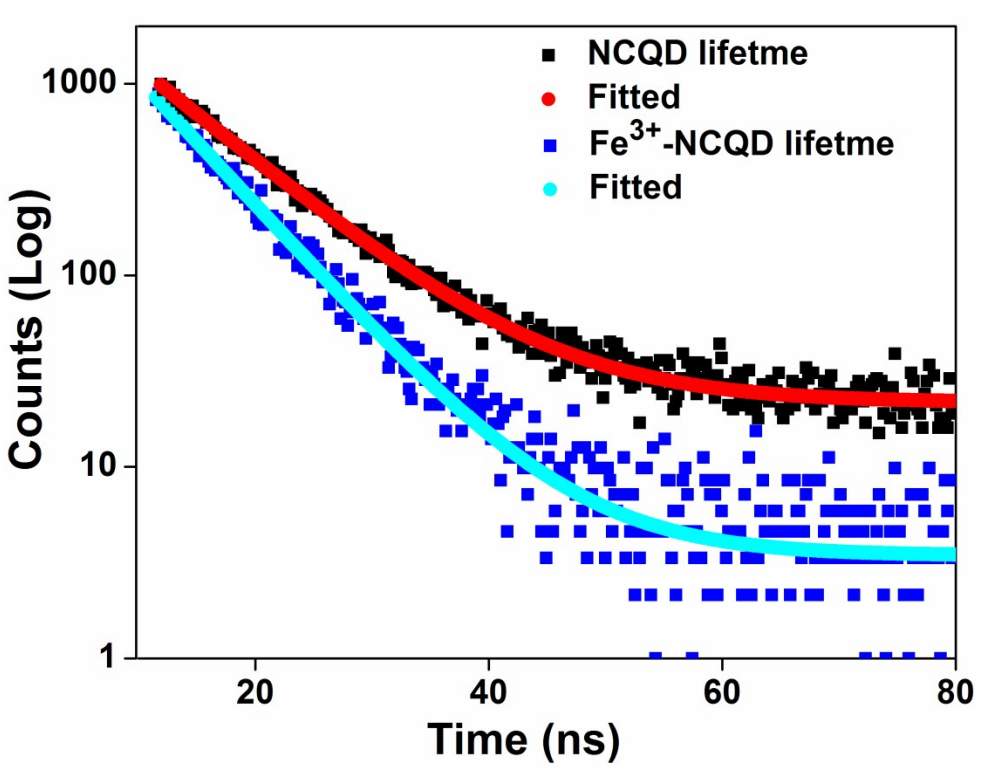

Figure S4: PL lifetime data of NCQD and Fe^{3+}-NCQD samples

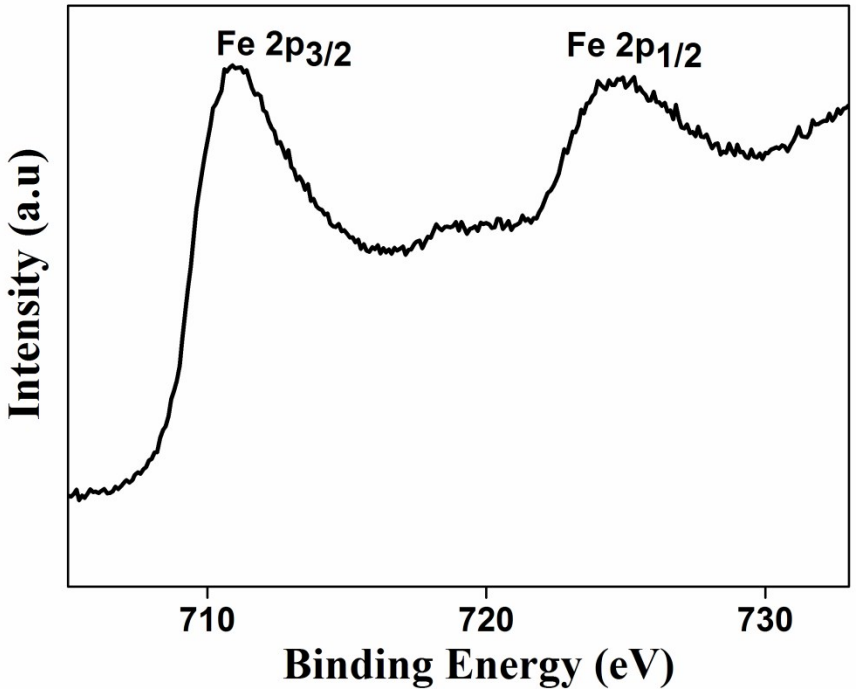

Figure S5: High resolution XPS peaks for Fe $2p_{3/2}$ and $Fe2p_{1/2}$

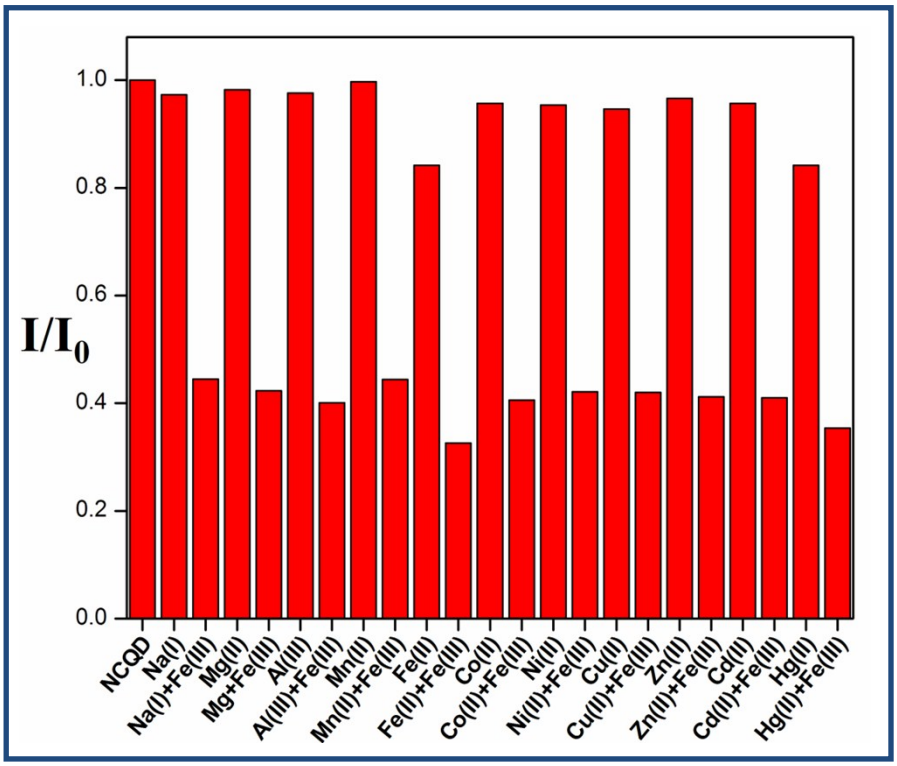

Figure S6: PL quenching efficiency of NCQD toward different metal ions and different metal in presence of Fe^{3+} ions at 140 μM

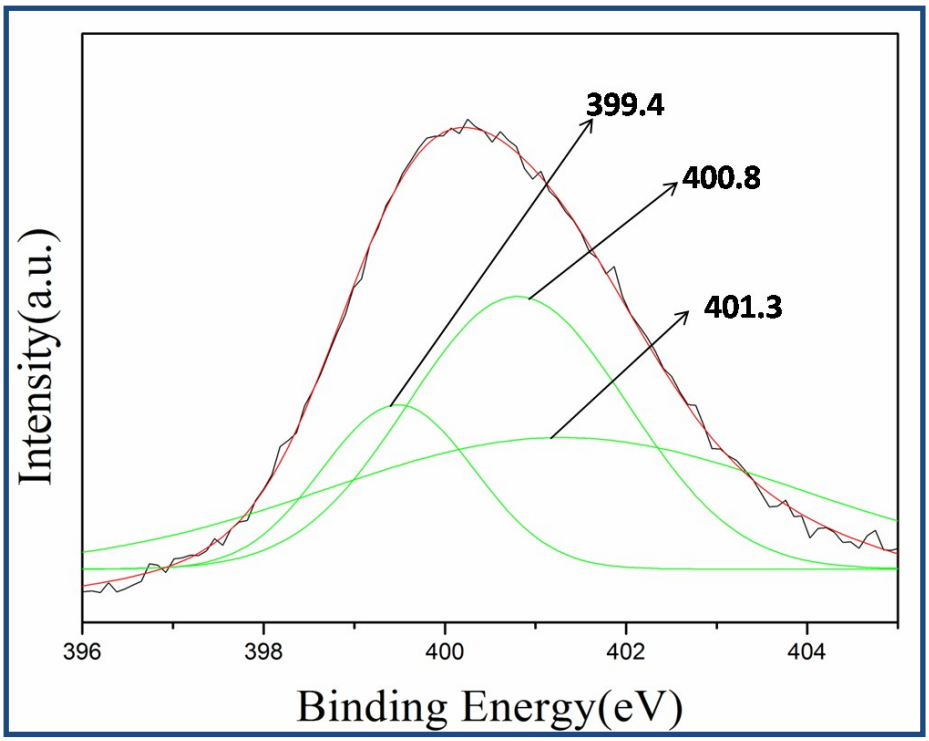

Figure S7: High resolution de-convoluted XPS peaks for N-1s of Fe (III)-NCQD

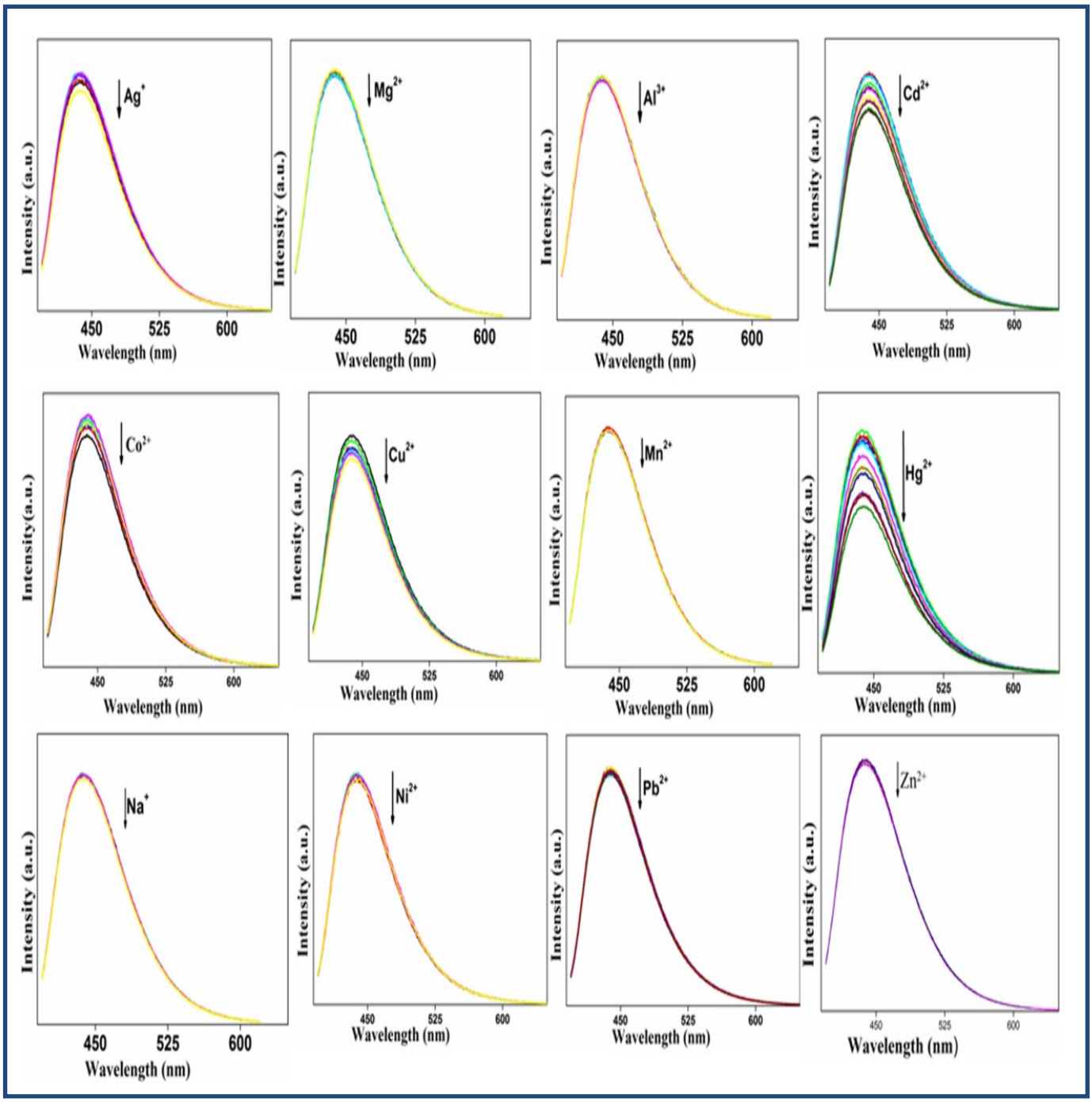

Figure S8: PL quenching of different metal ions- NCQD samples

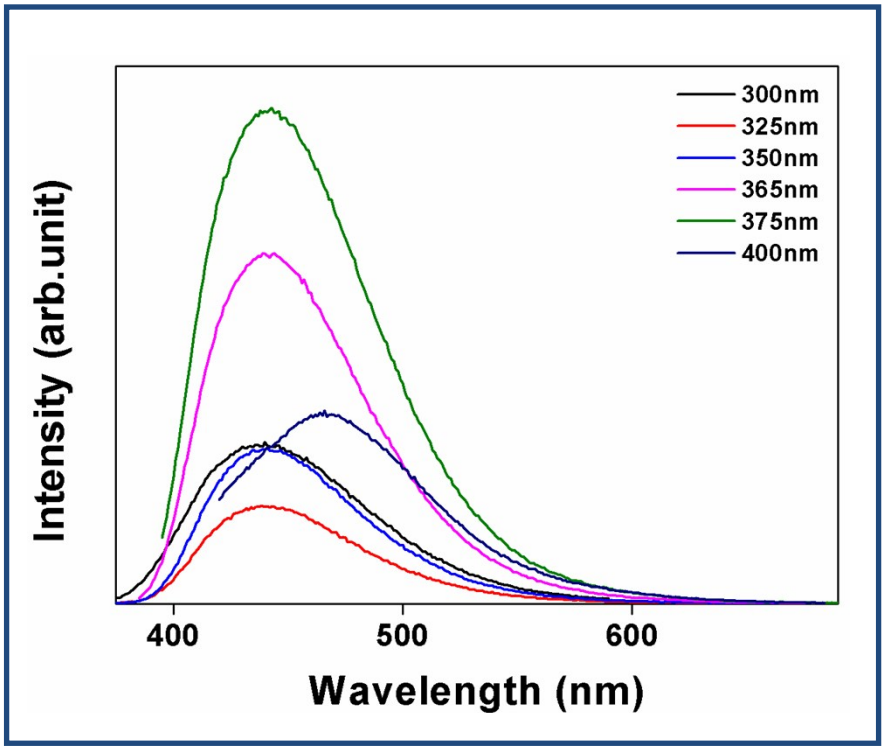

Figure S9: Excitation dependent PL spectra of exsitu NCQD in solution

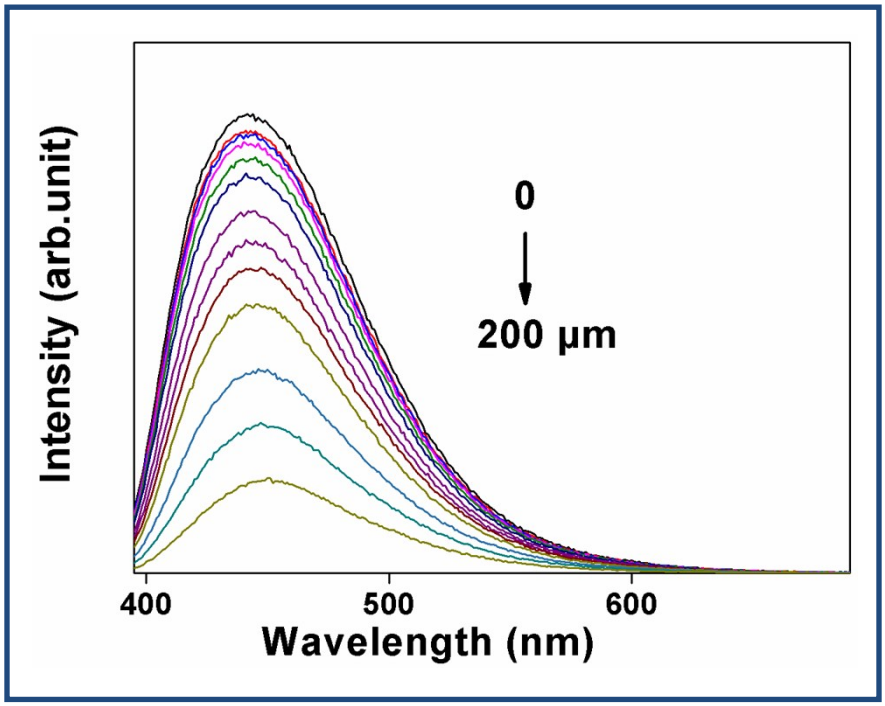

Figure S10: Fluorescence quenching of exsitu NCQD after gradual addition of different concentration of Fe^{3+} solution

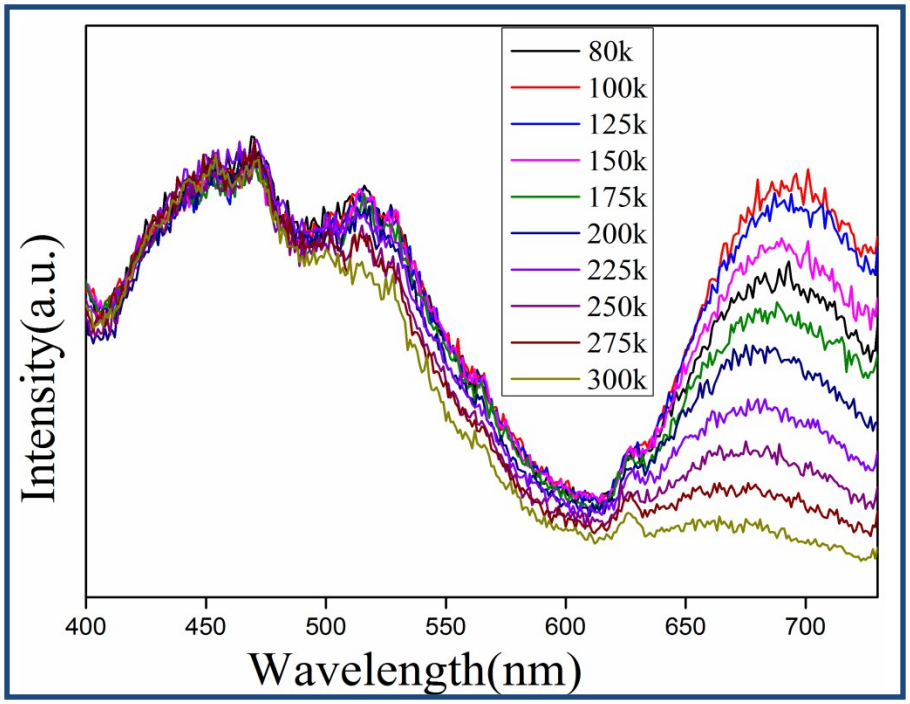

Figure S11: Temperature dependent PL spectra of exsitu NCQD film at 375nm excitation

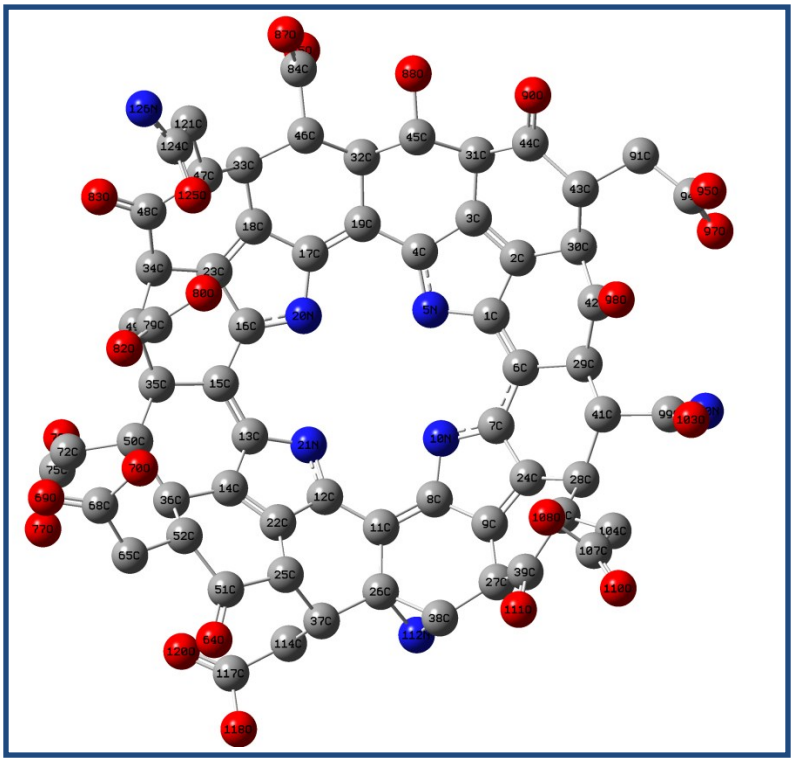

Figure S12: Optimized structure of NCQD core

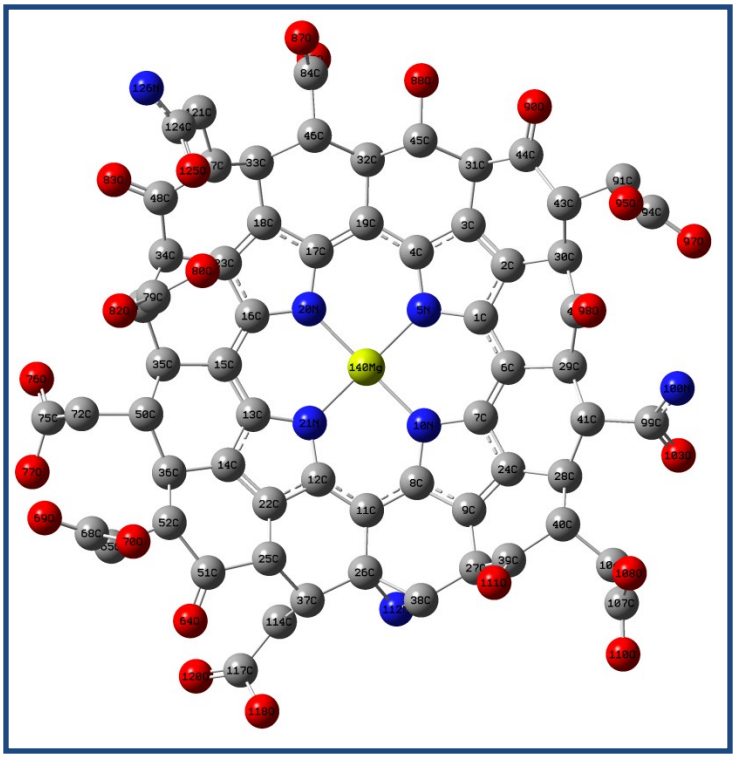

Figure S13: Optimized structure of magnesium (II) incorporated ring of NCQD core

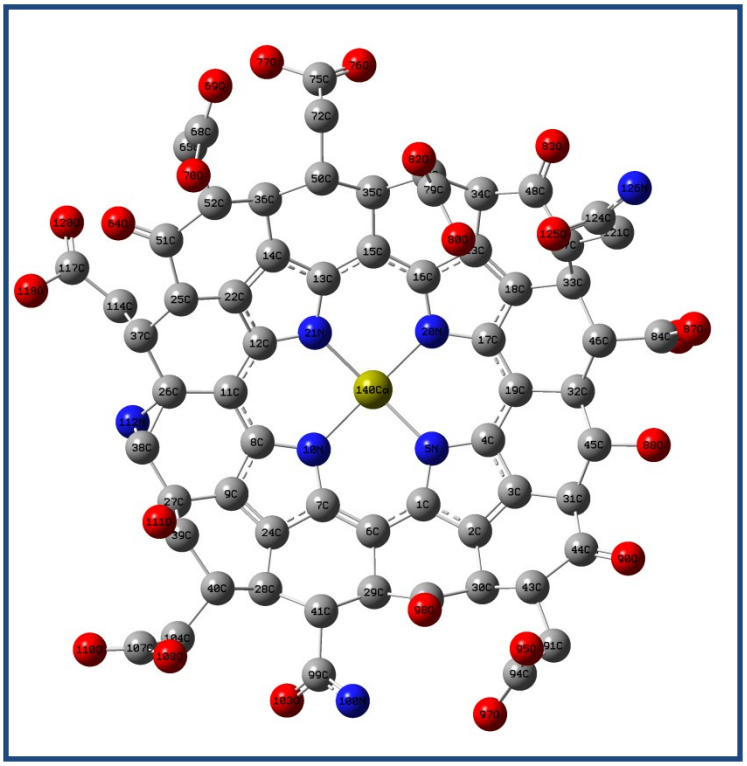

Figure S14: Optimized structure of calcium (II) incorporated ring of NCQD core

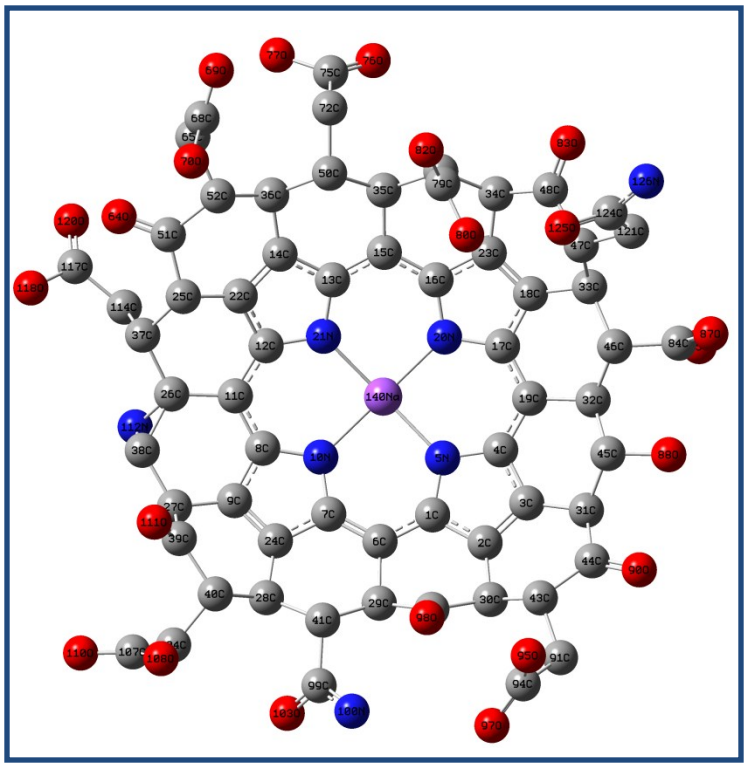

Figure S15: Optimized structure of sodium (I) incorporated ring of NCQD core

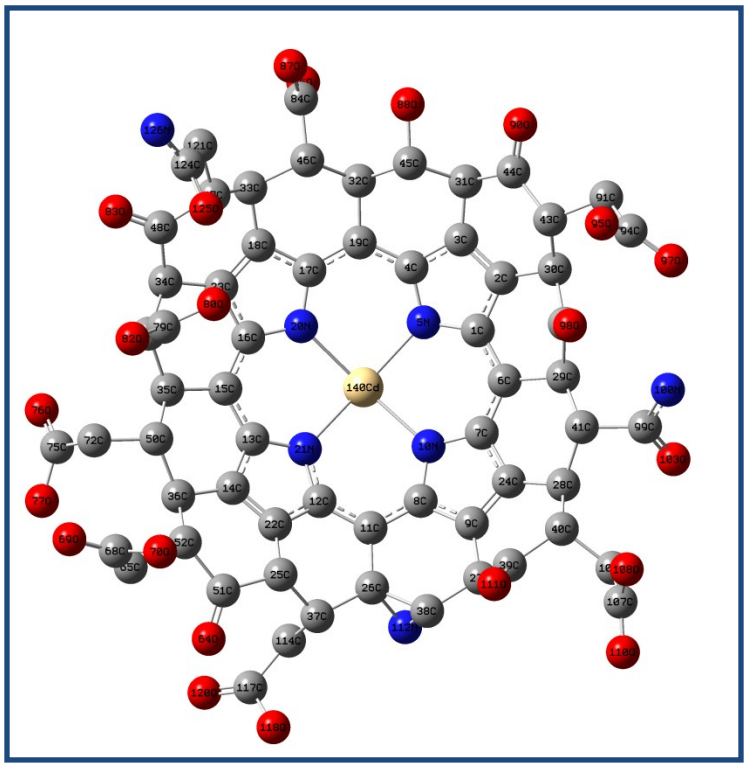

Figure S16: Optimized structure of cadmium (II) incorporated ring of NCQD core

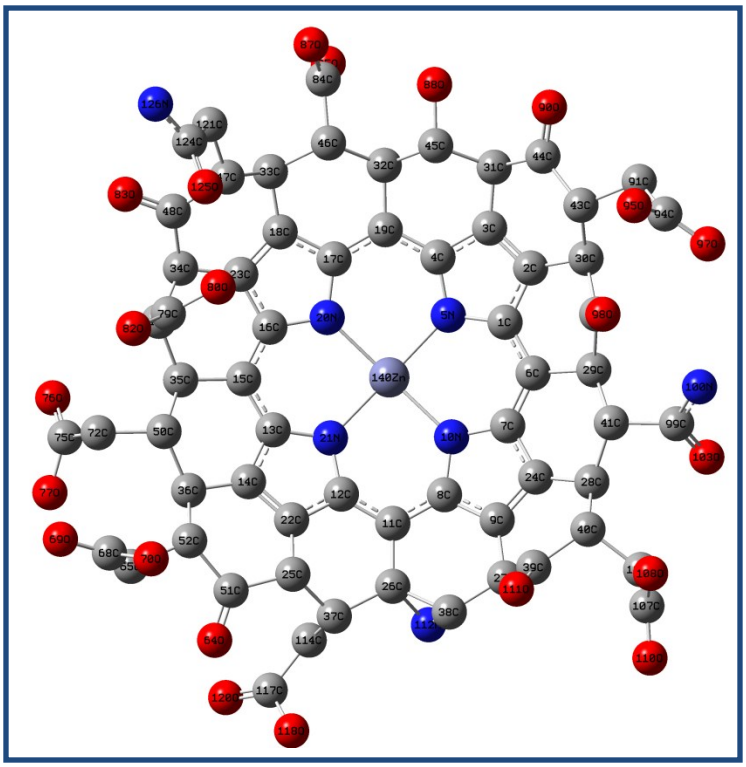

Figure S17: Optimized structure of zinc (II) incorporated ring of NCQD core

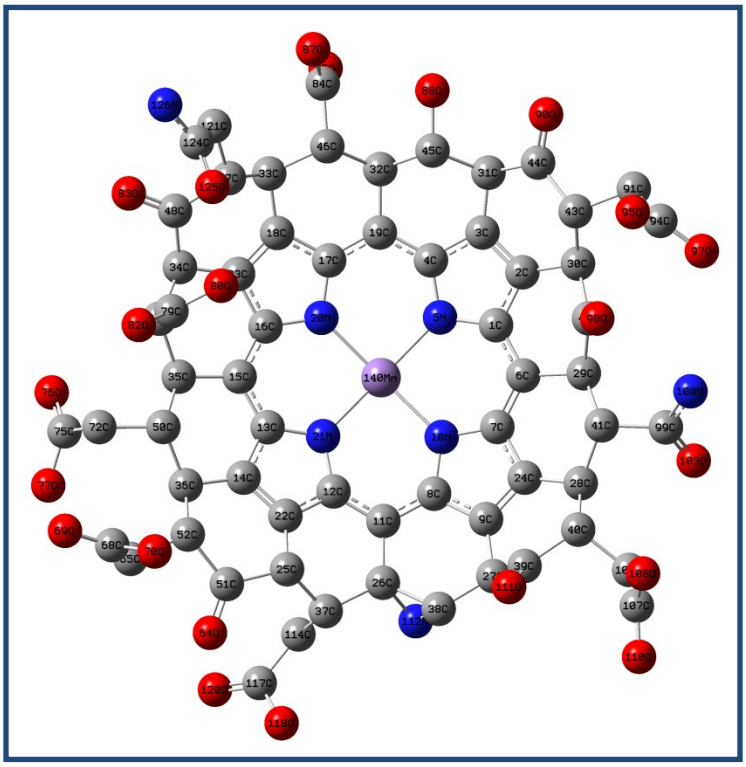

Figure S18: Optimized structure of manganese (II) incorporated ring of NCQD core

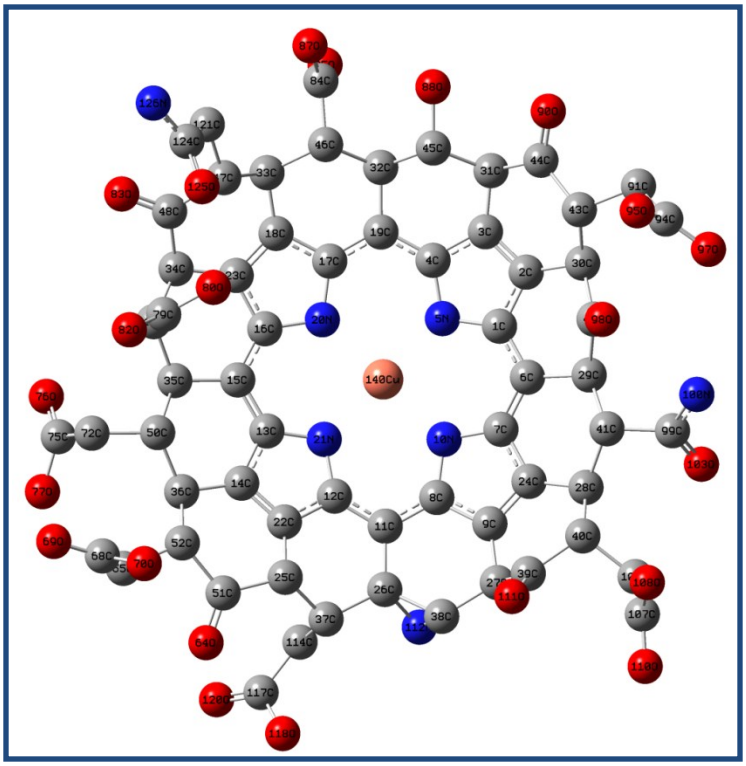

Figure S19: Optimized structure of Copper (II) incorporated ring of NCQD core

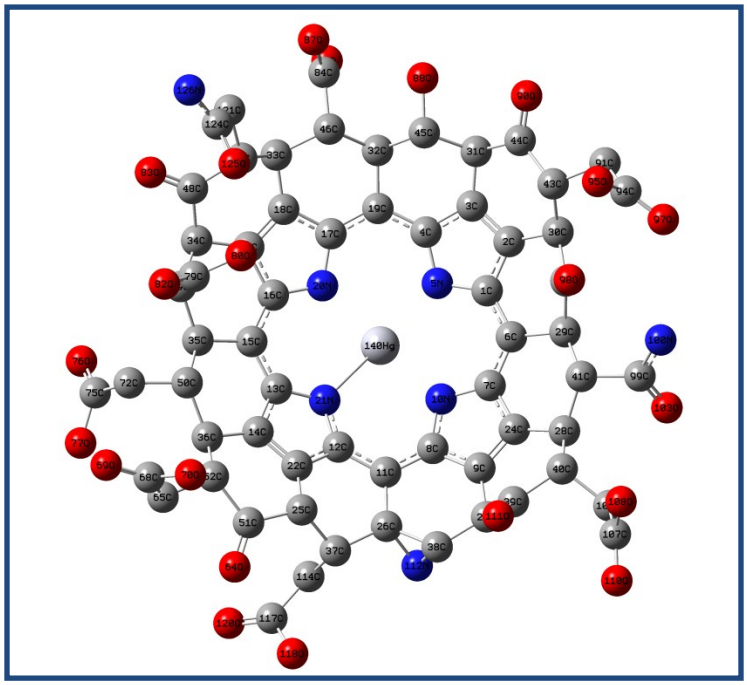

Figure S20: Optimized structure of Mercury (II) incorporated ring of NCQD core

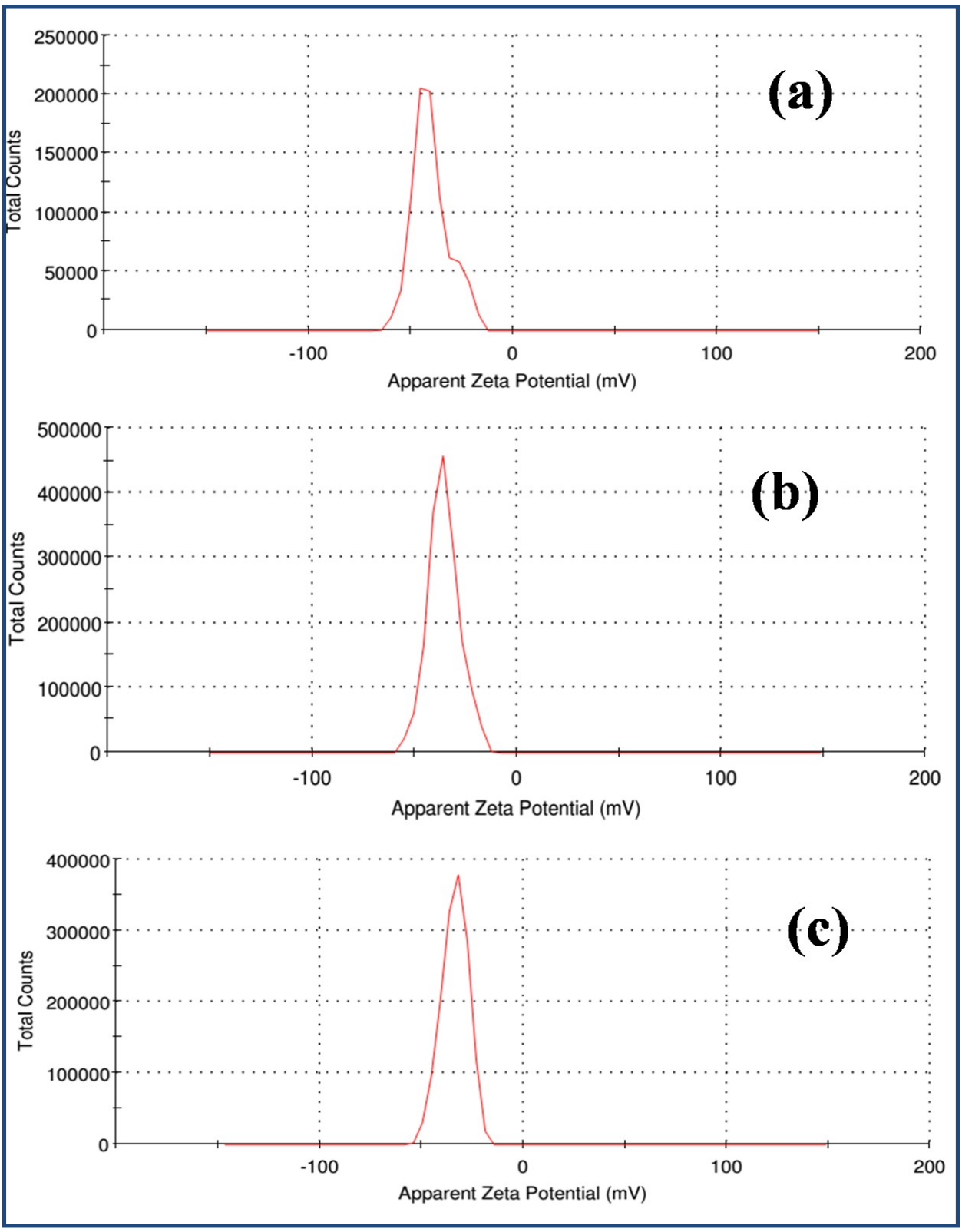

Figure S21: (a) Zeta potential of NCQD,(b) Zeta potential of Fe(II)-NCQD,(c) Zeta potential of Fe(III)-NCQD

Table S1: Basis sets and stabilization energies of bare and ion incorporated NCQD core with their optimized geometrical parameters:

Compounds	Basis set	Stabilization Energy (Kcal/mole)	Metal-N length (Å)
NCQD core		4.47	
With Fe	cc-pVDZ	5.73	1.960
Hg	lanl2dz	4.51	2.268
Cu	cc-pVDZ	4.66	2.004
Zn	cc-pVDZ	4.58	2.035
Cd	lanl2dz	4.51	2.197
Mn	cc-pVDZ	4.52	2.055
Ca	cc-pVDZ	4.61	2.122
Mg	cc-pVDZ	4.58	2.189
Na	cc-pVDZ	4.49	2.135

Table S2: Relative standard deviations (RSD) of various metal ions:

ions	RSD value	ions	RSD value
Fe	77.025±1.25%	Pb	3.042 ± 0.83%
Hg	31.6 ±2.89%	Ni	3.039 ± 0.71%
Cd	17.1 ±3.02%	Mg	3.04 ± 0.67%
Cu	10.231 ±0.77%	Al	2.027 ± 0.73%
Zn	9.057 ±1.70%	Mn	2.015 ± 0.46%
Co	8.1575±1.37%	Na	2.0155 ± 0.35%
Ag	8.1173 ±0.88%		